Elliptic flow of thermal photons in Au + Au collisions at $\sqrt{s_{NN}} = 200$ GeV

Fu-Ming Liu,[1] Tetsufumi Hirano,[2] Klaus Werner,[3] and Yan Zhu[4]
[1]*Institute of Particle Physics, Central China Normal University, Wuhan 430079, People's Republic of China*
[2]*Department of Physics, The University of Tokyo, Tokyo 113-0033, Japan*
[3]*Laboratoire SUBATECH, University of Nantes, IN2P3/CNRS, Ecole des Mines, Nantes, France*
[4]*Institute of Particle Physics, Central China Normal University, Wuhan, People's Republic of China*
(Received 17 August 2009; published 17 September 2009)

The transverse momentum (p_t) dependence, the centrality dependence, and the rapidity dependence of the elliptic flow of thermal photons in Au + Au collisions at $\sqrt{s_{NN}} = 200$ GeV are predicted on the basis of a three-dimensional ideal hydrodynamic description of the hot and dense matter. The elliptic flow parameter v_2, i.e., the second Fourier coefficient of azimuthal distribution, of thermal photons first increases with p_t and then decreases for $p_t > 2$ GeV/c, because of the weak transverse flow at the early stage. The p_t-integrated v_2 first increases with centrality, reaches a maximum at about 50% centrality, and then decreases. The rapidity dependence of the elliptic flow $v_2(y)$ of direct photons (mainly thermal photons) is very sensitive to the initial energy density distribution along the longitudinal direction, which provides a useful tool to extract the realistic initial condition from measurements.

DOI: 10.1103/PhysRevC.80.034905 PACS number(s): 25.75.−q, 12.38.Mh

I. INTRODUCTION

The deconfined and novel nuclear matter, quark-gluon plasma (QGP), has been expected to appear in relativistic heavy ion collisions. Various signatures have been proposed to verify its existence [1]. Many experiments have been done to explore the properties of QGP at the BNL Relativistic Heavy Ion Collider (RHIC) and will be done at the CERN Large Hadron Collider (LHC). Experimental results indicate that QGP has been created at the RHIC [2].

Collective flow, in particular elliptic flow, is an effective probe to use to investigate bulk properties of QGP in nucleus-nucleus collisions at relativistic energies. In noncentral collisions the overlapping reaction zone of two colliding nuclei has an anisotropic shape, like an almond, in the transverse plane. This leads to a preferred flow direction parallel to the impact parameter, and therefore the initial spatial anisotropy is carried over to momentum-space anisotropy [3]. The QGP created at the early stage expands, cools down, and finally forms a hadronic gas (HG) phase. Then hadrons still have strong rescatterings until freeze-out. Therefore those hadrons do carry information on the asymmetric flow, but only concerning the freeze-out surface.

Fortunately, in high energy heavy ion collisions, thermal photons can be produced during the whole history of the evolution of the hot and dense matter. Moreover the mean free path of photons is much larger than the transverse size of the bulk matter. So thermal photons produced in the interior of the plasma pass through the surrounding matter without any interaction. As a result, thermal photons provide information on flow asymmetries even from inside the bulk volume, not just on the surface.

In this article, we investigate the relation between the observables of thermal photons and the space-time evolution of the hot and dense matter for exploring QGP properties, based on a fully three-dimensional (3D) ideal hydrodynamic description of expansion of the matter. Toward establishment of the relation, we calculate the second Fourier coefficient of azimuthal momentum distribution, the so-called elliptic flow coefficient v_2, for thermal photons in Au + Au collisions at $\sqrt{s_{NN}} = 200$ GeV at various centralities (0–70%).

In Sec. II we briefly review the space-time evolution of the hot and dense matter using the 3D ideal hydrodynamics and the basic formula for the production of thermal photons. In Sec. III, we show our results on v_2 of thermal photons in Au + Au collisions at $\sqrt{s_{NN}} = 200$ GeV, its transverse momentum, centrality dependences, and rapidity dependence. Section IV is devoted to discussion and a summary of our results.

II. BULK EVOLUTION, THERMAL PHOTONS, AND ELLIPTIC FLOW

In our calculation, a full 3D ideal hydrodynamic calculation [4,5] is employed to describe the space-time evolution of the hot and dense matter created in Au + Au collisions at the RHIC. The local thermal equilibrium is assumed to be reached at the initial time $\tau_0 = 0.6$ fm/c. The transverse flow is assumed to be zero at τ_0. We consider two scenarios to obtain entropy density (or energy density) at τ_0: one is a parametrization based on the Glauber model [4,5] and the other is based on flux tubes (string picture) realized in the EPOS model [6]. For these two initial conditions, we take the same hydrodynamic equations and equations of state. The initial energy density from the two scenarios has been plotted as a function of space-time rapidity η_s in Fig. 1, where the dashed line refers to the parametrized initial conditions and the dotted line refers to the EPOS case. One can see that the energy density decreases very rapidly with η_s in the EPOS case, while it has a plateau for $|\eta_s| < 2.5$ using the parametrized initial conditions. In two-dimensional hydrodynamics this plateau is assumed for the whole η_s region. The EPOS initial condition gives many similar results compared to the parametrized ones;

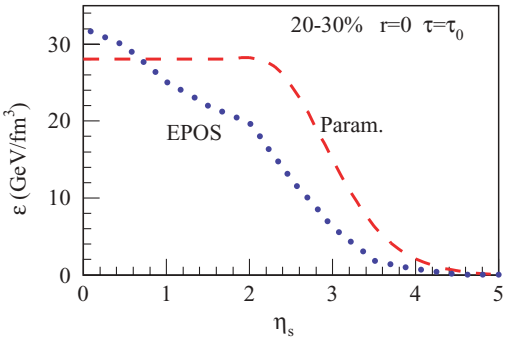

FIG. 1. (Color online) Energy density as a function of space-time η_s. The dashed line represents the parametrized initial conditions and the dotted line represents the EPOS initial conditions.

i.e., the measured p_t spectra of direct photons can also be well reproduced, and the same p_t dependence and centrality dependence of the elliptic flow of thermal photons has been observed. But there are also striking differences, which will be discussed later.

For both scenarios, the impact parameters corresponding to different centralities in Au + Au collisions at the RHIC are 3.2, 5.5, 7.2, 8.5, 9.7, 10.8, and 11.7 fm for 0–10%, 10–20%, . . . , and 60–70% centrality, respectively. The evolution of the fluid is governed by conservation laws of energy and momentum,

$$\partial_\mu T^{\mu\nu} = 0, \tag{1}$$

with the energy-momentum tensor

$$T^{\mu\nu} = (e + P)u^\mu u^\nu - P g^{\mu\nu} \tag{2}$$

for a perfect fluid. Here, e, P, and u^μ are energy density, pressure, and local four fluid velocity, respectively, which are related through the equation of state (EOS). The above equations are solved in full 3D space (τ, x, y, η_s), where τ, η_s, x, and y are the proper time, space-time rapidity, and the two transverse coordinates along the impact parameter and perpendicular to the reaction plane, respectively. Because the net-baryon density is small near the midrapidity at the RHIC, it is neglected. We also neglect the dissipative effects in the space-time evolution. The critical temperature of a first-order phase transition between the QGP phase and the hadron phase is fixed at $T_c = 170$ MeV. The EOS for the QGP phase is

$$P = \tfrac{1}{3}(e - 4B), \tag{3}$$

where the bag constant is tuned to $B^{\frac{1}{4}} = 247.19$ MeV so that the pressure of the QGP phase with three flavors is matched to that of the HG phase [up to mass of $\Delta(1232)$] at T_c. In the hadronic phase, we employ two resonance gas models: partial chemical equilibrium (PCE) and full chemical equilibrium (FCE) [5]. In the PCE model, the particle ratios including contributions from resonance decays are assumed to hold during the hadronic expansion, which is required from the data of particle ratios. The PCE model is our standard choice for calculating the photon spectra in the following. For the purpose of comparison, we also employ the conventional resonance gas model in which chemical equilibrium is maintained during the hadronic expansion. In both models, the hadronic matter is kinetically and thermally frozen at $e^{\rm th} = 0.08$ GeV/fm^3. The corresponding freeze-out temperature is $T^{\rm th} \sim 100(130)$ MeV for the PCE (FCE) model, which is consistent with the p_t slope of protons.

Transverse momentum spectra of thermal photons can be written as

$$\frac{dN}{dy\, d^2p_t} = \int d^4x\, \Gamma(E^*, T), \tag{4}$$

with $\Gamma(E^*, T)$ being the Lorentz invariant thermal photons' emission rate, which covers the contributions from the QGP phase [7] and the HG phase [8], $d^4x = \tau\, d\tau dx\, dy\, d\eta_s$ the volume element, and $E^* = p^\mu u_\mu$ the photon energy in the local rest frame. Here p^μ is the photons' four-momentum in the laboratory frame, T and u^μ are the temperature and the local fluid velocity, respectively, to be taken from the hydrodynamic calculations mentioned above. We only consider thermal photon radiation from the region with energy density above $e^{\rm th}$. For more details one can check [9] where the measured p_t spectra of direct photons at different centralities in Au + Au collisions are nicely reproduced.

The triple differential spectrum can be written as a Fourier series,

$$\frac{d^3N}{dy\, d^2p_t} = \frac{d^2N}{2\pi p_t\, dp_t\, dy}\left(1 + \sum_{n=1}^{\infty} 2v_n \cos(n\phi)\right), \tag{5}$$

where ϕ is the azimuthal angle of the photons' momentum with respect to the reaction plane, which is defined to be the plane containing the impact parameter and beam axis. The elliptic flow is quantified by the second harmonic coefficient v_2,

$$v_2(p_t, y) = \frac{\int d\phi \cos(2\phi) d^3N/dy\, d^2p_t}{\int d\phi d^3N/dy\, d^2p_t}. \tag{6}$$

The p_t dependence of the triple differential spectra is strongly affected by the flow u through the argument $E^* = p^\mu u_\mu$ in the photon emission rate. In the local rest frame thermal photons of any given energy are emitted isotropically. The isotropic distribution is Lorentz-boosted by the flow velocity $\vec{v}_r$. The azimuthal asymmetry of the transverse components of the flow obviously ends up with an anisotropic momentum distribution, which gives a finite v_2. Therefore both strength and the anisotropy of transverse flow velocity are important to generate the elliptic flow of thermal photons. To understand

TABLE I. The strength and the anisotropy of the transverse flow at each centrality.

Centrality (%)	0–10	10–20	20–30	30–40	40–50	50–60	60–70
$\langle v_r \rangle$	0.114	0.122	0.123	0.117	0.109	0.0959	0.0804
$\langle v_2^{\rm hydro} \rangle$	0.0417	0.103	0.154	0.188	0.212	0.222	0.240

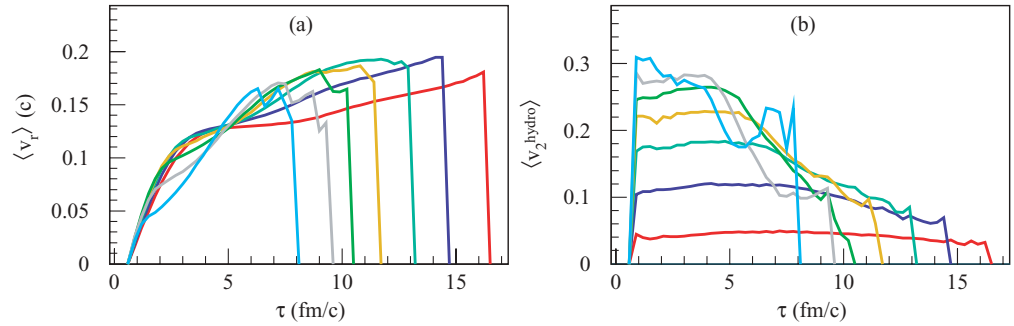

FIG. 2. (Color online) Average radial flow velocity (a) and average flow anisotropy (b) as a function of proper time. Different curves correspond to 0–10%, 10–20%, . . . , 60–70%, respectively. A line with a longer life time represents the corresponding result for a more central collision.

the thermal photon v_2 quantitatively, we define the mean radial flow $\langle v_r \rangle$ and the mean anisotropy of flow $\langle v_2^{\rm hydro} \rangle$ as

$$\langle v_r \rangle = \left\langle \sqrt{v_x^2 + v_y^2} \right\rangle \tag{7}$$

$$\left\langle v_2^{\rm hydro} \right\rangle = \langle \cos 2\phi_v \rangle = \left\langle \frac{v_x^2 - v_y^2}{v_x^2 + v_y^2} \right\rangle, \tag{8}$$

where $\langle \cdots \rangle$ stands for energy-density-weighted space-time average, v_x and v_y are the flow velocity components along the x axis and the y axis, respectively. We only consider the region above $e = e^{\rm th} = 0.08$ GeV/fm^3, where thermal photons are produced in this model.

From Table I, we see that the mean radial flow increases with centrality from 0–10% ($b = 3.2$ fm) to 20–30% ($b = 7.2$ fm), then decreases from 20–30% ($b = 7.2$ fm) to 60–70% ($b = 11.7$ fm). On the other hand, the mean flow anisotropy increases with centrality from 0–10% to 60–70% monotonically. One can easily understand the tendency when we investigate the time evolution of space-averaged results in Figs. 2(a) and 2(b). One should notice that, for all centralities, the average radial flow is quite small before $\tau = 1$ fm/c, during which most of thermal photons in $4 < p_{\rm t} < 6$ GeV/c are produced.

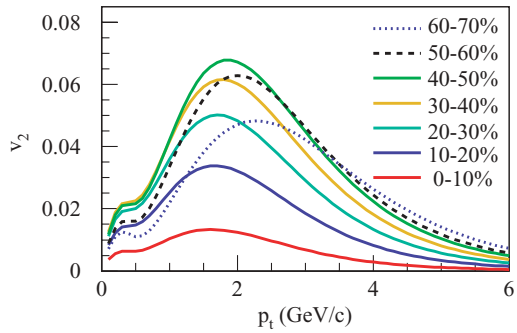

FIG. 3. (Color online) v_2 for thermal photons in Au + Au collisions at $\sqrt{s_{NN}} = 200$ GeV is shown for various centralities from 0 to 70% in $0 < p_t < 6$ GeV/c. The solid lines from bottom to top correspond to the centralities 0–10%, 10–20%, 20–30%, 30–40%, and 40–50%, respectively. The dashed lines from top to bottom at $p_t = 2$ GeV/c correspond to the centralities 50–60% and 60–70%.

III. RESULTS

In Fig. 3, the v_2 of thermal photons in $0 < p_t < 6$ GeV/c is shown for various centralities from 0 to 70% in Au + Au collisions at $\sqrt{s_{NN}} = 200$ GeV. The solid lines from bottom to top refer to the centralities 0–10%, 10–20%, 20–30%, 30–40%, and 40–50%, respectively. The dashed lines from top to bottom at $p_t = 2$ GeV/c refer to the centralities 50–60% and 60–70%.

For each centrality, the thermal v_2 increases then decreases with increasing p_t and a peak appears at $p_t \sim 2$ GeV/c. The same p_t dependence has been predicted in the study with 2 + 1D ideal hydrodynamics [10]. The decrease of thermal photons' v_2 at high p_t can be explained as the weak transverse flow at the early stage. Because at the higher p_t, the fraction of thermal photons emitted from the hot matter at an early stage is greater for all centralities; i.e., at $p_t = 3$ GeV/c, about 50% thermal photons are produced during $\tau \in (0.6, 0.9)$ fm/c, and at $p_t = 4$ GeV/c, the fraction is about 70%. In our 3 + 1D hydrodynamics, the evolution of the radial flow is plotted in Fig. 2(a). At an early time near τ_0, i.e., $\tau \in (0.6, 0.9)$ fm/c, the transverse flow vanishes, and so does the elliptic flow of thermal photons. Therefore, the decrease of thermal photons' $v_2(p_t)$ at high p_t reflects the weak transverse radial flow in the early stage. Note that a similar nontrivial behavior is also seen in p_t slope parameters of dimuon spectra as a function of invariant mass [11].

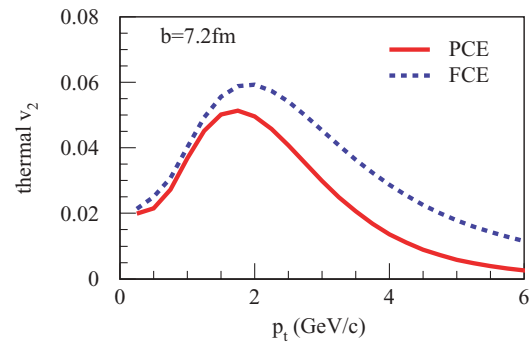

FIG. 4. (Color online) The elliptic flow of thermal photons at $b = 7.2$ fm. Solid (dashed) line is the result from a partial chemical equilibrium model (a full chemical equilibrium model).

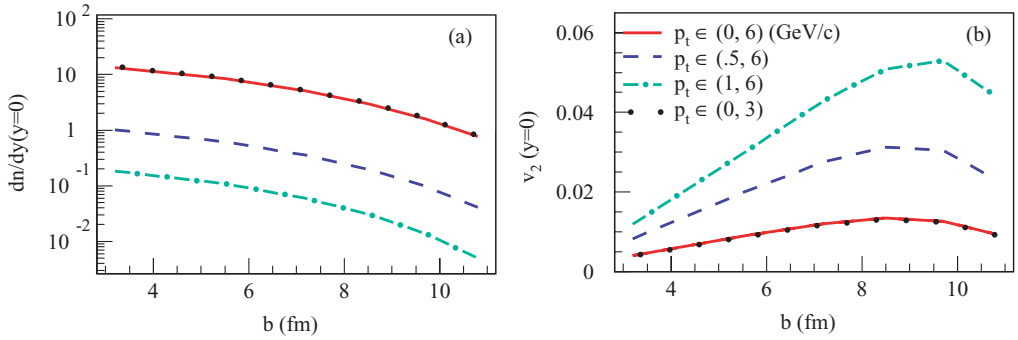

FIG. 5. (Color online) (a) The yield and (b) the v_2 of thermal photons at midrapidity. Different curve types represent different p_t-integral ranges, i.e., (0,3) GeV/c, dotted lines; (0,6) GeV/c, solid lines; (0.5,6) GeV/c, dashed lines; (1,6) GeV/c, dashed-dotted lines.

Similar to the 2 + 1D hydrodynamics [10], small bumps appear in the elliptic flow of thermal photons at p_t close to zero. This is because the thermal photons are emitted from two phases, the QGP phase and the hadronic phase, at different times. In fact, the thermal photon emission rate [7] is not reliable at $p_t \to 0$.

One can also see an EOS dependence of the thermal photon elliptic flow. As an example, we change from the PCE model to the FCE model, which has been employed in the conventional hydrodynamic calculations including the thermal photon calculations in early study [11]. The change of the EOS is almost invisible in the p_t spectra of thermal photons because of the dominant contribution from the QGP phase. However, the $v_2(p_t)$ from the hadronic phase is about ten times bigger than the one from the QGP phase. So a slight change in the hadronic phase can be magnified and become quite visible in the elliptic flow of thermal photons, as shown in Fig. 4. One can also conclude that the elliptic flow of thermal photons is sensitive to the EOS, particularly in the hadron phase. However, the effect of the different EOS we obtained here is quite similar to the effect from the different formation time of quark-gluon plasma [12].

The centrality dependence has been investigated in Fig. 5, where panel (a) represents the yield and panel (b) the v_2 of thermal photons at midrapidity, and where different types of curves present different p_t ranges. It is clear that the yield of thermal photons decreases with centrality monotonously. However, the elliptic flow of thermal photons does not change with centrality monotonously. It reaches a maximum at impact parameter $b = 9.7$ fm or 40–50% centrality and then decreases for more central or more peripheral collisions, because of the interplay between the strength and the anisotropy of the transverse flow. As we discussed in Sec. II, both the strength and the anisotropy of transverse flow are important factors to generate the elliptic flow of thermal photons. The anisotropy increases with decreasing centrality, but the strength of the transverse flow decreases, as shown in Table I.

In Fig. 5 the p_t ranges used are (0,3) GeV/c, dotted lines; (0,6) GeV/c, solid lines; (0.5, 6) GeV/c, dashed lines; and (1,6) GeV/c, dashed-dotted lines. One can see the yield and the p_t-integrate v_2 of thermal photons are not sensitive to the upper limit, c.f. the integral ranges (0,3) and (0,6) GeV. This is clear because the p_t spectrum of thermal photons decreases almost exponentially and the high p_t region contributes very little to the total yield. The p_t spectrum of direct photons is dominated by the thermal photons at the low p_t region and also decreases rapidly with p_t. So we can expect that the p_t-integrated quantities of direct photons behave similarly to those of thermal photons. However, one can see that the yield and the p_t-integrated v_2 of thermal photons are very sensitive to the lower limit, because of the rapidly decreasing p_t spectrum. One should be careful when a comparison between the prediction and the measurement is performed because the lower limit is experimentally determined by the detectors.

The above results are all at midrapidity. In the following we discuss the rapidity dependence for the two scenarios: initial

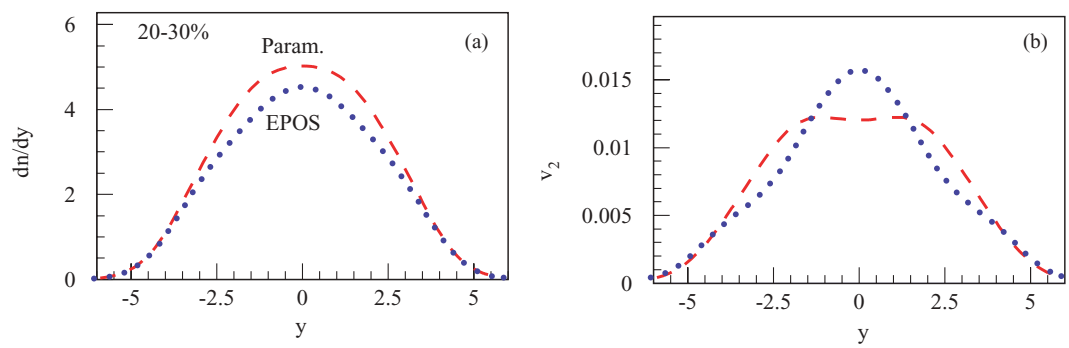

FIG. 6. (Color online) (a) Rapidity dependence of thermal photon production. (b) Rapidity dependence of the p_t-integrated v_2 of thermal photons. Dashed lines are from the parametrized initial conditions and the dotted lines are from the EPOS initial conditions.

conditions based on EPOS flux tubes and the parametrized initial conditions. As already said, both scenarios give many similar results. However, the rapidity dependence of the elliptic flow is very different. In Fig. 6, the rapidity distributions of dn/dy and the v_2 of thermal photons produced from the two kinds of initial conditions are shown. The dashed lines represent the parameterized initial conditions and the dotted lines represent the EPOS initial conditions. One can see the thermal photon yield dn/dy has a similar dependence on rapidity y, but two very different dependences of the elliptic flow $v_2(y)$ have been obtained. One can see that $v_2(y)$ shows almost the same shape as the initial $\epsilon(\eta_s)$: A rapid decrease of elliptic flow along longitudinal direction is obtained from EPOS initial conditions, where the energy density decreases very rapidly with η_s, while a plateau of $v_2(y)$ at the midrapidity region is obtained from the parametrized initial conditions. A similar observation has already been made concerning the rapidity dependence of the elliptical flow of hadrons [6].

IV. DISCUSSION AND CONCLUSION

On the basis of a fully three-dimensional ideal hydrodynamic description of the evolution of the hot and dense matter created in Au + Au collisions at $\sqrt{s_{NN}} = 200$ GeV, we found that the elliptic flow of thermal photons depends nontrivially on not only the anisotropy but also the strength of the transverse flow.

At midrapidity, the v_2 of thermal photons increases with p_t up to $p_t \sim 2$ GeV/c and then decreases at higher p_t, similar to the prediction from two-dimensional ideal hydrodynamics [10]. The decrease of thermal photons' v_2 at high p_t reflects the fact that at very early times the transverse radial flow is weak. Therefore thermal photons can serve as a penetrating and unique probe for the whole history of the evolution.

The p_t-integrated v_2 of thermal photons increases with increasing impact parameter b up to ∼10 fm (40–50% centrality) and then decreases above that. Thermal photons from two different phases have the same centrality dependence. The decrease of thermal photons' v_2 at peripheral collisions is the result of the interplay between the strength and the anisotropy of the transverse radial flow of the hot matter. As impact parameter b increases, the anisotropy increases, but the strength of transverse radial flow decreases.

The rapidity dependence of the elliptic flow of thermal photons' $v_2(y)$ can "remember" the initial energy density along the longitudinal direction $\epsilon_0(\eta_s)$; i.e., a plateau at midrapidity can be obtained from the parametrized initial conditions based on the Glauber model, whereas a rapid decrease of the elliptic flow along rapidity is obtained from the EPOS initial conditions.

ACKNOWLEDGMENTS

This work is supported by the Natural Science Foundation of China under Project No. 10505010 and MOE of China under Project No. IRT0624. The work of T.H. was partly supported by Grant-in-Aid for Scientific Research No. 19740130 and by Sumitomo Foundation No. 080734.

[1] J. W. Harris and B. Müller, Annu. Rev. Nucl. Part. Sci. **46**, 71 (1996), and references therein.
[2] I. Arsene *et al.* (BRAHMS Collaboration), Nucl. Phys. **A757**, 1 (2005); B. B. Back *et al.* (PHOBOS Collaboration), *ibid.* **A757**, 28 (2005); J. Adams *et al.* (STAR Collaboration), *ibid.* **A757**, 102 (2005); K. Adcox *et al.* (PHENIX Collaboration), *ibid.* **A757**, 184 (2005).
[3] J. Y. Ollitrault, Phys. Rev. D **46**, 229 (1992); **48**, 1132 (1993).
[4] T. Hirano, Phys. Rev. C **65**, 011901(R) (2001).
[5] T. Hirano and K. Tsuda, Phys. Rev. C **66**, 054905 (2002).
[6] K. Werner, T. Hirano, Iu. Karpenko, T. Pierog, S. Porteboeuf, M. Bleicher, and S. Haussler, J. Phys. G: Nucl. Part. Phys. **36**, 064030 (2009).
[7] P. Arnold, G. Moore, and L. G. Yaffe, J. High Energy Phys. 01 (2001) 057; 12 (2001) 009.
[8] S. Turbide, R. Rapp, and C. Gale, Phys. Rev. C **69**, 014903 (2004).
[9] F. M. Liu, T. Hirano, K. Werner, and Y. Zhu, Phys. Rev. C **79**, 014905 (2009).
[10] R. Chatterjee, E. S Frodermann, U. Heinz, and D. K. Srivastava, Phys. Rev. Lett. **96**, 202302 (2006).
[11] J. E. Alam, T. Hirano, J. K. Nayak, and B. Sinha, arXiv:0902.0446 [nucl-th].
[12] R. Chatterjee and D. K. Srivastava, Phys. Rev. C **79**, 021901 (2009).